AEDC-TR-76-53

ARCHIVE COPY
DO NOT LOAN

STAGNATION POINT SOLUTION OF VISCOUS SHOCK LAYER EQUATIONS FOR FLOW PAST A SPHERE

DEPARTMENT OF AEROSPACE ENGINEERING
UNIVERSITY OF CINCINNATI
CINCINNATI, OHIO 45221

August 1976

Final Report for Period April 1974 to March 1976

Approved for public release; distribution unlimited.

AEDC TECHNICAL LIBRARY
5 0720 00062 3191

Property of U. S. Air Force
AEDC LIBRARY
F40600-75-C-0001

Prepared for

DIRECTORATE OF TECHNOLOGY
ARNOLD ENGINEERING DEVELOPMENT CENTER
ARNOLD AIR FORCE STATION, TENNESSEE 37389

NOTICES

When U. S. Government drawings specifications, or other data are used for any purpose other than a definitely related Government procurement operation, the Government thereby incurs no responsibility nor any obligation whatsoever, and the fact that the Government may have formulated, furnished, or in any way supplied the said drawings, specifications, or other data, is not to be regarded by implication or otherwise, or in any manner licensing the holder or any other person or corporation, or conveying any rights or permission to manufacture, use, or sell any patented invention that may in any way be related thereto.

Qualified users may obtain copies of this report from the Defense Documentation Center.

References to named commercial products in this report are not to be considered in any sense as an endorsement of the product by the United States Air Force or the Government.

This final report was submitted by Department of Aerospace Engineering, University of Cincinnati, Cincinnati, Ohio 45221, under contract F40600-74-C-0011, with the Arnold Engineering Development Center (DYR), Arnold Air Force Station, Tennessee 37389. Elton R. Thompson, DYR, was the AEDC Project Engineer.

This report has been reviewed by the Information Office (OI) and is releasable to the National Technical Information Service (NTIS). At NTIS, it will be available to the general public, including foreign nations.

APPROVAL STATEMENT

This technical report has been reviewed and is approved for publication.

FOR THE COMMANDER

Elton R. Thompson

ELTON R. THOMPSON
Research & Development
Division
Directorate of Technology

Robert O. Dietz

ROBERT O. DIETZ
Director of Technology

REPORT DOCUMENTATION PAGE		READ INSTRUCTIONS BEFORE COMPLETING FORM
1. REPORT NUMBER AEDC-TR-76-53	2. GOVT ACCESSION NO.	3. RECIPIENT'S CATALOG NUMBER
4. TITLE (and Subtitle) STAGNATION POINT SOLUTION OF VISCOUS SHOCK LAYER EQUATIONS FOR FLOW PAST A SPHERE		5. TYPE OF REPORT & PERIOD COVERED Final Report - April 1974 to March 1976 6. PERFORMING ORG. REPORT NUMBER AFL 76-4-20
7. AUTHOR(s) B. N. Srivastava, M. J. Werle, and R. T. Davis		8. CONTRACT OR GRANT NUMBER(s) F40600-74-C-0011
9. PERFORMING ORGANIZATION NAME AND ADDRESS Aerospace Engineering Department University of Cincinnati Cincinnati, Ohio 45221		10. PROGRAM ELEMENT, PROJECT, TASK AREA & WORK UNIT NUMBERS Program Element 65807F
11. CONTROLLING OFFICE NAME AND ADDRESS Arnold Engineering Development Center(DYFS) Air Force Systems Command Arnold Air Force Station, Tennessee 37389		12. REPORT DATE August 1976 13. NUMBER OF PAGES 31
14. MONITORING AGENCY NAME & ADDRESS(if different from Controlling Office)		15. SECURITY CLASS. (of this report) UNCLASSIFIED 15a. DECLASSIFICATION/DOWNGRADING SCHEDULE N/A

16. DISTRIBUTION STATEMENT (of this Report)

Approved for public release; distribution unlimited.

17. DISTRIBUTION STATEMENT (of the abstract entered in Block 20, if different from Report)

1. Spheres -- Shock waves
2. " -- Hypersonic flow

18. SUPPLEMENTARY NOTES

Available in DDC

19. KEY WORDS (Continue on reverse side if necessary and identify by block number)

spheres	equations
blunt bodies	stagnation point
fluid flow	supersonic flow
shock (mechanics)	hypersonic flow
layers	hypervelocity

20. ABSTRACT (Continue on reverse side if necessary and identify by block number)

Numerical solutions in the stagnation region of a spherically blunted body are obtained by using the full and thin layer version of the viscous shock layer equations. The numerical system utilizes an implicit finite difference scheme combined with a relaxation technique for determining the bow shock shape. Comparisons with experimental data are made for shock Reynolds numbers, Re_s, of 20 to 2000 and Mach numbers of 4 to 20. Both the surface

DD FORM 1 JAN 73 1473 EDITION OF 1 NOV 65 IS OBSOLETE

20. ABSTRACT (Continued)

heating levels as well as the shock layer density profiles are presented. It is found that with the inclusion of the shock and body slip, the full viscous shock layer model apparently enjoys a range of validity down to Re_s of 20 to 30. The thin layer version of these equations are shown to be inadequate for such low Reynolds numbers.

AFSC
Arnold AFS Tenn

PREFACE

The results reported herein were obtained for the Arnold Engineering Development Center by the University of Cincinnati, Department of Aerospace Engineering under Contract F40600-74-C-0011. The authors of this report were B. N. Srivastava, M. J. Werle, and R. T. Davis. The Air Force Project Engineer for this contract was E. R. Thompson, AEDC/DYR. The Program Element Number was 65807F.

This report covers the work during the period April 1974 to March 1976. The reproducibles used in the reproduction of this report were supplied by the authors.

TABLE OF CONTENTS

		Page
I.	Introduction	5
II.	Governing Equations for the Viscous Shock Layer	5
III.	Numerical Analysis	8
IV.	Results and Discussion	9
V.	Conclusions	13
VI.	References	14

LIST OF FIGURES

Figure		Page
1	Coordinate System	17
2	Stagnation Point Heat Transfer	18
3	Further Comparison of Stagnation Point Heat Transfer	19
4	Shock Wave and Sonic Line Locations for a Spherical Body	20
5	Variation of Stanton Number With Reynolds Number for Thin Layer.	21
6	Variation of Stanton Number with Reynolds Number for Full Layer.	22
7	Stagnation Point Density Profiles	
	(A) RE = 129	23
	(B) RE = 50	24
	(C) RE = 24	25
8	Stagnation Point Density Profiles	
	(A) RE = 358	26
	(B) RE = 96	27
	(C) RE = 37	28
9	Stagnation Point Temperature Profile	29
NOMENCLATURE.		30

I. INTRODUCTION

The reentry problem continues to provide motivation for study of low Reynolds number high Mach number blunt body flows. This flow regime is one in which the viscous effects influence a significant portion of the total shock layer thickness, thereby violating the classical boundary layer approximations and requiring the use of a more comprehensive set of governing equations. Such a set are the viscous shock layer equations (Refs. 1 and 2) which represent an intermediate level of approximation between the boundary layer and Navier-Stokes equations. These equations contain all of the terms in the Navier-Stokes equations which contribute to second order boundary layer theory plus those which arise to second order in the outer inviscid portion of the shock layer. Although some evidence exists that the viscous shock layer model will suffice for reentry type flow problems (Refs. 3 and 4), there has, as yet, not been a critical assessment of the range of validity of these equations. This situation is due to the difficulties involved in solution of these equations. Although several methods have been presented for solving the "thin" shock layer approximation to these more general equations (Refs. 5 and 6), such approaches suffer two limitations. First, they are based on the assumption that the pressure gradients normal to the body surface are established entirely by centrifugal effects, and second, that the shock wave lies parallel to the body surface. In an attempt to remove these limitations, methods have been developed (see Refs. 7 and 8) for addressing the full shock layer equations through a relaxation process wherein the thin shock layer assumptions are removed by iteration. However, no attempt has been made, as yet, to assess the range of validity of these equations. This is performed in the present work through comparison with experimental stagnation point data for spherical nose shapes. Numerical solutions of the viscous shock layer equations are obtained by combining an implicit finite difference scheme with a relaxation technique for determining the bow shock shape (see Ref. 7). The effects of thin layer approximations, wall slip and shock slip boundary conditions are included in the analysis to establish their relative importance.

II. GOVERNING EQUATIONS FOR THE VISCOUS SHOCK LAYER

The governing equations are written in a boundary-layer coordinate system (see Fig. 1). The equations and notations used are the same as those used by Davis (Ref. 1) or Srivastava, Werle and Davis (Ref. 9).

Continuity Equation:

$$[(r + n\cos\phi)^J \rho u]_s + [(1 + kn)(r + n\cos\phi)^J \rho v]_n = 0 \qquad (1)$$

s-Momentum Equation:

$$\rho\{u[u_s/(1 + kn)] + v\, u_n + [k/(1 + kn)]uv\} + p_s/(1 + kn)$$

$$= [\varepsilon^2/(1 + kn)^2(r + n\cos\phi)^J][(1 + kn)^2(r + n\cos\phi)^J\tau]_n \tag{2}$$

where

$$\tau = \mu[u_n - ku/(1 + kn)] \tag{3}$$

n-Momentum Equation:

$$\rho\{u[v_s/(1 + kn)] + vv_n - [k/(1 + kn)]u^2\} + p_n = 0 \tag{4}$$

where with the thin shock layer approximation, equation (4) becomes,

$$p_n = [k/(1 + kn)]\rho\, u^2 \tag{5}$$

Energy Equation:

$$\rho\{u[T_s/(1 + kn)] + v\, T_n\} - \{u[p_s/(1 + kn)] + v\, p_n\}$$

$$= [\varepsilon^2/(1 + kn)(r + n\cos\phi)^J][(1 + kn)(r + n\cos\phi)^J q]_n$$

$$+ (\varepsilon^2/\mu)\tau^2 \tag{6}$$

where $q = (\mu/\sigma)T_n$ (7)

Equation of State:

$$p = [(\gamma-1)/\gamma]T\rho \tag{8}$$

Viscosity Law

$$\mu = [(1 + c')/(T + c')]T^{3/2} \tag{9}$$

$$c' = c^*/(\gamma - 1)M_\infty^2\, T_\infty^* \tag{10}$$

where c^* is taken to be 198.6°R for air.

Surface slip conditions consistant with the approximations used in the above set of equations are given as

$$\left.\begin{aligned} v &= 0 && (11a)\\ u &= \varepsilon^2\, a_1 (1/p)\{[(\gamma-1)/\gamma]T\}^{1/2}\,\tau && (11b)\\ p &= p_w + \varepsilon^2\, b_1 (\sigma/T)\{[(\gamma-1)/\gamma]T\}^{1/2}\, q && (11c)\\ T &= T_w + \varepsilon^2\, c_1 (\sigma/p)\{[(\gamma-1)/\gamma]T\}^{1/2}\, q && (11d) \end{aligned}\right\} \text{ at } n = 0$$

where τ and q are given by equations (3) and (7).

Conditions at the shock surface are obtained using the concept of "shock slip" to represent the usual higher order Reynolds number effects on the shock compression process. This gives modified Rankine-Hugoniot relations as shown:

$$u_{sh} = u^1_{sh} \sin(\alpha+\beta) + v^1_{sh} \cos(\alpha+\beta) \tag{12}$$

$$v_{sh} = - u^1_{sh} \cos(\alpha+\beta) + v^1_{sh} \sin(\alpha+\beta) \tag{13}$$

where u^1_{sh} and v^1_{sh} are the components of velocity tangent and normal to the shock interface, respectively, and are given along with the temperature, pressure and density from the following expressions:

$$\rho_{sh}\, v^1_{sh} = - \sin\alpha \tag{14}$$

$$\varepsilon^2\, \mu_{sh} (u^1_n)_{sh} + \sin\alpha\, u^1_{sh} = \sin\alpha \cos\alpha \tag{15}$$

$$\begin{aligned} &\varepsilon^2\, \sigma^{-1}\, \mu_{sh}\, (T_n)_{sh} + \sin\alpha\, T_{sh} - (\sin\alpha/2)(u^1_{sh} - \cos\alpha)^2 \\ &\quad = \sin\alpha/2\, \{[4\gamma/(\gamma+1)^2]\sin^2\alpha + [2/(\gamma-1) - 4(\gamma-1)/(\gamma+1)^2]1/M^2_\infty \\ &\quad - 4/(\gamma+1)^2\, M^4_\infty \sin^2\alpha\} \end{aligned} \tag{16}$$

$$p_{sh} = [2/(\gamma+1)]\sin^2\alpha - (\gamma-1)/\gamma(\gamma+1)M_\infty^2 \tag{17}$$

$$\rho_{sh} = \gamma\ p_{sh}/(\gamma-1)T_{sh} \tag{18}$$

For reasons discussed in Reference (1) the above equations were solved here after the independent and dependent variables were normalized by their corresponding shock values. The resulting set of governing equations and the boundary conditions are given in Reference (1).

III. NUMERICAL ANALYSIS

This set of viscous shock layer equations is of the parabolic-hyperbolic type and is therefore solved using a method similar to that used for solving the boundary layer equations, such as the method of Blottner and Flugge-Lotz (Ref. 10). The calculation of the shock shape, though, represents an elliptic effect. To properly account for the shock shape, the present method of solution adopted a relaxation technique wherein the shock slope was determined iteratively. After each pass along the body surface a least squares Chebyshev polynomial was used to smooth the numerically calculated shock shape over the entire range of integration in the downstream direction. This method of solution was found to work well for flow past blunt bodies where the shock stand off distance is not small and the shock shape differs significantly from the body shape. For a detailed description of the numerical method one is referred to Reference (9).

The overall method of solution employed is as follows:

An initial guess was made on the shock slope. This was done by giving initial values to the coefficients of the Chebyshev polynomial which represents the shock slope function. The equations were then solved by starting with the stagnation point where they reduce to a set of ordinary differential equations. The first equation solved was the energy equation so that thereafter all quantities such as viscosity related to temperature could be evaluated. Next the s-momentum equation was integrated to determine a $\bar{u}$ velocity profile, and then the continuity equation was solved to determine first the shock stand off distance from equation (39a) (Ref. 9), and then the $\bar{v}$ component of velocity from equation (31) (Ref. 9). Finally equation (33) (Ref. 9) was integrated to determine the local pressure level.

Repetition of the above steps at a given station continued until the solution converged. The method then stepped along the body surface and iterated at each station to achieve converged solutions. To accelerate the convergence process, the previous station values of the profiles were used at each new step as a first guess. Once the above method had passed over the entire mesh, the coefficients of the Chebyshev polynomials were recalculated using the calculated values of the shock derivative at every station. The entire procedure was repeated until the coefficients of the Chebyshev polynomial converged to a desired accuracy.

The solutions so obtained were labeled as "Thin Shock Layer" solutions when the approximate normal momentum equation (Eqn. 5) was used. Further solutions using the more correct normal momentum equation (Eqn. 4) were obtained by a similar procedure. These solutions were labeled as "Full Shock Layer" solutions. However for this phase of calculations the $\bar{v}$ terms in the normal momentum equation were used from the previous iteration.

The shock slip conditions were handled by evaluating the $(u_n^1)_{sh}$ and $(T_n)_{sh}$ terms from the previous step in the iteration and then solving the resulting equation for this shock condition.

IV. RESULTS AND DISCUSSION

Figure (2) presents a comparison of normalized stagnation point heating on spheres with experimental data and other theoretical results. The numerical calculations were made at a free stream Mach number, M_∞, of 8, a wall to stagnation temperature ratio of 0.25 and a total temperature of 500°R. The heat flux in figure (2) is normalized with its value obtained from a boundary layer analysis at the same test conditions. Note that the full layer results rightfully approach unity as Reynolds number increases in good agreement with the higher order boundary layer theory of Van Dyke (Ref. 21) that gives

$$q/q_{B.L.} \rightarrow 1 + 0.866/\sqrt{Re_s}$$

Comparison of the present full shock layer results (including shock and wall slip effects) with the experimental data of Potter and Miller (Ref. 11), Wittliff and Wilson (Ref. 12) and Hickman (Ref. 13) is good over the entire Reynolds number range.

Figure (2) also shows the analytical result of Cheng (Ref. 6) where a Newtonian thin shock layer approach was employed. Both wall and shock slip effects were incorporated in these solutions and thus, are seen to compare favorably with the present calculations over the entire Reynolds number range.

In an effort to assess the importance of wall and shock slip conditions on the predicted results, solutions were also obtained without slip effects included. As shown in figure (2) as the Reynolds number decreases, wall slip effects become important and then shock slip effects grow to a significant level. Both these effects are of equal significance in the low Reynolds number regime.

It is also noted from figure (2) that while the full shock layer equations yield results that compare well with various data, their thin layer approximations give results that are significantly lower than the data for the Reynolds number range shown.

However, note should be made that the data of Ferri et. al. (Ref. 14) which were obtained with $M_\infty = 8$, $T_w/T_o = 0.25$ and $T_o = 2300°R$, was found to be higher than those predicted by any of the other analytical or experimental results. Hickman (Ref. 13) attributed this apparent increase to the higher stagnation temperature level of Ferri's experimental conditions (2300°R) as compared to his test stagnation temperature level of 500°R. In order to clarify this situation another set of numerical calculations were made where the test conditions were taken to be the same as those used by Ferri et. al. (Ref. 14). The results of such a calculation is shown in Figure (3). It is noted from this figure that when the stagnation temperature of the test condition is increased from 540°R, as used by Hickman (Ref. 13), to 2300°R corresponding to the test case of Ferri et. al. (Ref. 14), the stagnation point heating levels do not show much influence. Hence the difference between the data of Ferri et. al. (Ref. 14) and the present calculations remains, as yet, unexplained.

In order to further test the viscous shock layer model, numerical calculations were made corresponding to the theoretical calculations of Dellinger (Ref. 5) at a free stream Mach number, M_∞, of 14.3, a free stream Reynolds number, Re_∞, of 3200 and a wall to stagnation temperature ratio of 0.0282. Figure (4) presents the shock wave and sonic line locations for this case. The results from the present analysis compare well with the calculations of Dellinger and with the inviscid blunt body solution of Van Dyke and Gordon (Ref. 15). The apparent descrepancy in the location of the sonic line between the present results and the inviscid results of Van Dyke and Gordon (Ref. 15)

near the shock is due to the fact that the present results are for a Mach number of 14.3 as against 10 used by Van Dyke and Gordon (Ref. 15). The difference near the body is due to the viscous effects which cause the Mach number to be lower than inviscid theory would predict. Thus the results obtained at this test condition are seen to be reasonably good.

Further test data, such as those due to Boylan (Ref. 16) are available at the higher free stream Mach number of 21.0, than those shown in Figure (2). Figure (5) shows the Stanton number at the stagnation point corresponding to the test data ($M_\infty = 21$, $T_w/T_o = 0.11$) of Boylan (Ref. 16). The theoretical calculations shown in this figure were obtained using the "thin layer" version of the full shock layer equations. It is noted that these equations correctly predict the qualitative behavior of the stagnation point Stanton number with increasing altitude, however the quantitative values are seen to be significantly different from those of the data. This difference is seen in Figure (5) to reduce, first with the inclusion of the effects of wall slip, and then further with the inclusion of the effect of shock slip. The influence of the slip is seen to be smaller at lower altitudes, as seen also in Figure (2). Hence the "thin layer" version of the full shock layer equations would not predict correct physical properties at lower Reynolds numbers. However, as seen in Figure (6), the full layer equations without slip effects included are observed to give as erroneous results as their "thin layer" counterpart. These equations are seen to give reasonably good results only when both wall and shock slip effects are included. Thus, the effects of slip are seen to be large in the lower Reynolds number regime and must be accounted for.

In order to assess the capability of the present model to represent the full flow structure across the shock layer, comparison is made in Figure (7) with the density profile measured by Russel (Ref. 17) for flow of nitrogen past a sphere at various free stream Reynolds numbers. Figure (7a) shows the density profile corresponding to a shock Reynolds number of 129 and a free stream Mach number of 4.11. The experimental result shows a finite thickness of the shock wave whose effect on the shock layer density is seen to be correctly modeled using the present approach. It is noted that the shock discontinuity modeled in the present analysis rightly occurs in the middle of the shock thickness shown by the experimental data. This figure also shows the results of Jain and Adimurthy (Ref. 18) where solutions were obtained using a series truncation technique of the Navier Stokes equations in the stagnation region. While their results well model the shock layer region, they apparently misrepresent the shock wave region due to the fact that the series truncation approach tacitly assumes the shock to be spherical over the entire stagnation region. The "thin layer" version of these equations are also seen to yield results that compare well with the data. It is noted from this figure that the

effects of wall and shock slip are not large so far as comparison with density profile data is concerned, however these effects are seen to cause a significant change in the wall properties. Thus, care must be taken to include these effects in the proper regime.

Figure (7b) shows the density profile corresponding to Russel's data of a free stream Mach number of 4.19 and a shock Reynolds number of 50. These results show that with the decreasing shock Reynolds number the density profile predicted by "thin" and "full" shock layer equations are significantly different. Further decrease in shock Reynolds number causes a large difference between the density profile predicted by the full shock layer equations and their "thin layer" counterpart as shown in Figure (7c) where the test conditions were taken to be a free stream Mach number, of 4.38 and a shock Reynolds number of 24.0. The experimental data in this figure shows a comparatively larger shock wave region than that seen in Figures (7a) or (7b), however the viscous shock layer model predicts the density profile reasonably well. The slip effects are noted to have a significant influence on the predicted density profile at this low shock Reynolds number case. Thus it is observed from these figures that when the full shock layer equations are used including the effects of slip, the predicted density profile compares well with the experimental data for a wide range of shock Reynolds numbers.

The density profiles discussed above were obtained for a diatomic gas such as nitrogen for which the ratio of specific heats were taken to be 1.4. Further test data were also considered for a monotomic gas such as argon where the ratio of specific heats were taken to be 1.667. Figures (8a,b,c) show the density profiles for such a gas for various free stream Reynolds numbers corresponding to the test condition of Russel (Ref. 17). Figure (8a) shows the density profile for a shock Reynolds number of 358 and a Mach number of 3.94. The predicted results compare well with the data and the effects of thin layer approximations and slip are not significant in a region away from the wall. However these effects grow to a significant level as the shock Reynolds number is decreased to a value of 96.0, as shown in Figure (8b), and further to a value of 37.0 as shown in figure (8c). No different outcome thus, is observed when the gas model is changed from a diatomic gas to a monotomic gas. As a final comparison, Figure (9) shows the temperature profile on the stagnation line of a spherical body at $M_\infty = 19$, $T_w/T_o = 0.19$ and $Re_s = 54.0$ measured by Ahouse and Bogdonoff (Ref. 19) along with various other theoretical calculations. The results obtained by the present analysis only compare qualitatively with the experimental data, but they do show a trend similar to the shock layer analysis of Cheng (Ref. 6) and the Navier-Stokes analysis of Li (Ref. 20).

Note that, even though the similarity solution of Jain and Adimurthy (Ref. 18) tacitly assumes the shock to be spherical in the nose region, their results seem to be surprisingly closer to the experimental data. The exact source of the discrepancy between the present shock layer analysis and the experimental data in the outer reaches of the layer is as yet unexplained.

In an overall sense, the results obtained here indicate that the viscous shock layer model compares well with experimental data to very low Reynolds numbers. It is found that with the inclusion of the shock and body slip, the full viscous shock layer model apparently enjoys a range of validity down to shock Reynolds numbers on the order of 20-30.

V. CONCLUSIONS

A finite difference method, where solutions are obtained using a least square Chebyshev polynomial to fit the numerically determined shock shape (Ref. 7), has been successfully applied to the solution of the viscous shock layer equations for flow past a sphere. Solutions so obtained were used to establish the range of validity of these equations by comparison with various experimental data. Based on these comparisons it is believed that the full shock layer model when used along with the wall and shock slip conditions apparently enjoy a range of validity down to shock Reynolds numbers on the order of 20 to 30. The calculated surface heating levels and the shock layer profiles are seen to be in good agreement with the various experimental and theoretical results. The approach in the present analysis is seen to well represent the shock wave location and other physical quantities of the flow. It is further determined that the thin layer version of these equations are inadequate for low values of the shock Reynolds numbers.

VI. REFERENCES

1. Davis, R.T., "Numerical Solution of the Hypersonic Viscous Shock Layer Equations," AIAA Journal, Vol. 8, No. 5, May 1970, pp. 843-851.

2. Davis, R.T., "Hypersonic Flow of a Chemically Reacting Binary Mixture Past a Blunt Body," AIAA Paper No. 70-805.

3. Anderson, E.C. and Moss, J.N., "Numerical Solution of the Steady-State Navier-Stokes Equations for Hypersonic Flow About Blunt Axisymmetric Bodies," NASA TMX-71977, 1973.

4. Miner, E.W. and Lewis, C.H., "Hypersonic Ionizing Air Viscous Shock-Layer Flows Over Sphere Cones," AIAA Journal, January 1975, pp. 80-88.

5. Dellinger, T.C., "Nonequilibrium Air Ionization in Hypersonic Fully Viscous Shock Layers," AIAA Paper No. 70-806, June 1970.

6. Cheng, H.K., "The Blunt-Body Problem in Hypersonic Flow at Low Reynolds Number," Report AF-1285-A-10, 1963, Cornell Aeronautical Laboratory.

7. Davis, R.T. and Nei, Y.W., "Numerical Solution of the Viscous Shock Layer Equations for Flow Past Spheres and Paraboloids," Final Report, Sandia Corporation, Contract No. 48-9195.

8. Werle, M.J., Srivastava, B.N. and Davis, R.T., "Numerical Solutions to the Full Viscous Shock Layer Equations Using an ADI Technique," Report No. AFL 74-7-13, Department of Aerospace Engineering, University of Cincinnati, August 1974.

9. Srivastava, B.N., Werle, M.J., and Davis, R.T., "Solution of the Hypersonic Viscous Shock Layer Equations for Flow Past a Paraboloid," Report No. AFL-74-4-10, Department of Aerospace Engineering, University of Cincinnati, April 1974.

10. Blottner, F.G. and Flügge-Lotz, I., "Finite Difference Computation of the Boundary Layer With Displacement Thickness Interaction," Journal de Mecanque, Vol. II, No. 4, 1963.

11. Potter, L.J. and Miller, J.T., "Total Heating Load on Blunt Axisymmetric Bodies in Low Density Flow," AIAA Journal, Vol. 1, pp. 480-481, 1963.

12. Wittliff, C.E. and Wilson, M.R., "Low Density Stagnation Point Heat Transfer in the Hypersonic Shock Tunnels," ARS Journal, Vol. 32, pp. 275-276, 1962.

13. Hickman, R.S., "The Influence of Shock Wave Boundary Layer Interaction on Heat Transfer to an Axisymmetric Body," Technical Report No. HE-150-191, Series No. 191, Issue No. 1, August 1962, University of California, Institute of Engineering Research, Berkeley, California.

14. Ferri, A., Zakkay, V. and Ting, L., "Blunt Body Heat Transfer at Hypersonic Speed and Low Reynolds Numbers," Journal of Aerospace Sciences, December 1962, pp. 962-971.

15. Van Dyke, M.D. and Gordon, H.D., "Supersonic Flow Past a Family of Blunt Axisymmetric Bodies," NASA TR-R-1, 1959.

16. Boylan, D.E., "Laminar Convective Heat-Transfer Rates on a Hemisphere Cylinder in Rarefied Hypersonic Flow," AIAA Journal, Vol. 9, No. 8, August 1971, pp. 1661-1663.

17. Russel, D.A., "Density Ahead of Sphere in Rarefied Supersonic Flow," The Physics of Fluids, Vol. 11, No. 8, 1968, pp. 1679-1685.

18. Jain, A.C. and Adimurthy, V., "Hypersonic Merged Stagnation Shock Layers, Part II, Cold Wall Case," AIAA Journal, Vol. 12, No. 3, March 1974, pp. 348-354.

19. Ahouse, D.R. and Bogdonoff, S.M., "An Experimental Flow Field Study of the Rarefied Blunt-Body Problem," AIAA Paper 69-656, San Francisco, California, 1969.

20. Li, C.P., "Hypersonic Nonequilibrium Flow Past a Sphere at Low Reynolds Numbers," AIAA Paper No. 74-173, Washington, D.C., February 1974.

21. Van Dyke, M. "Second Order Boundary Layer Theory With Application to Blunt Bodies in Hypersonic Flow," AFOSR-TN-61-1270, 1961.

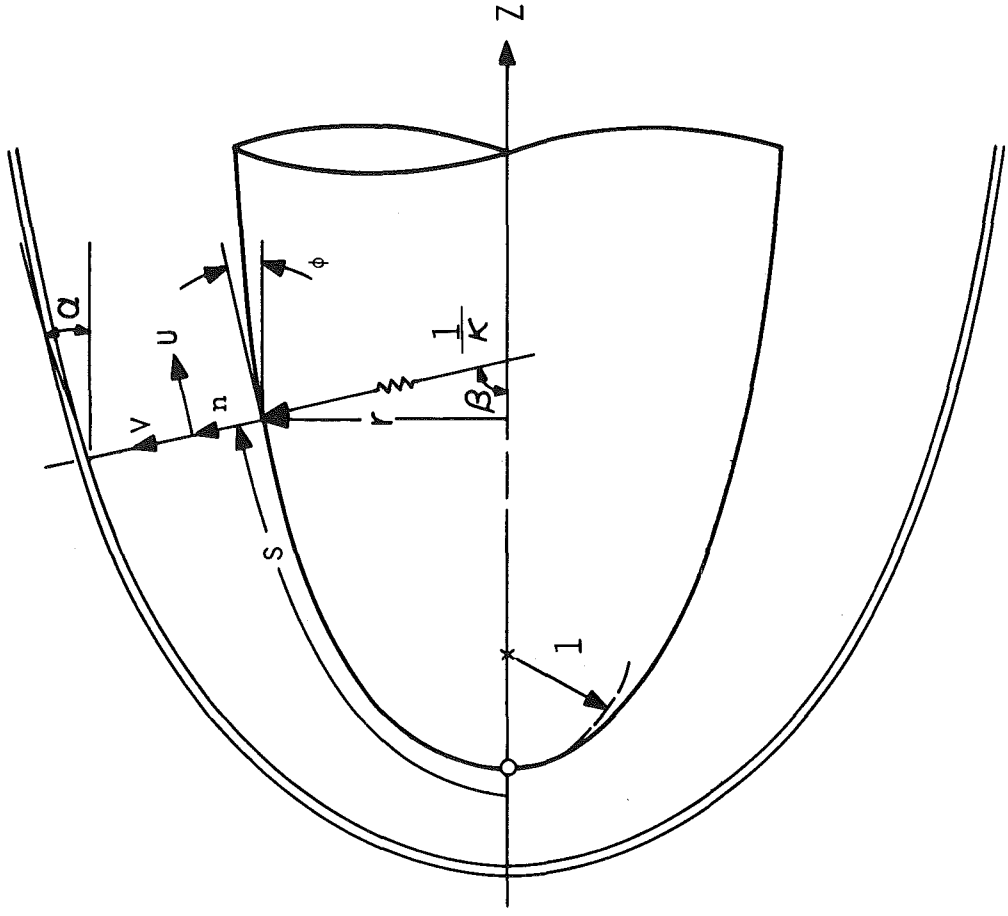

Figure 1. Coordinate system.

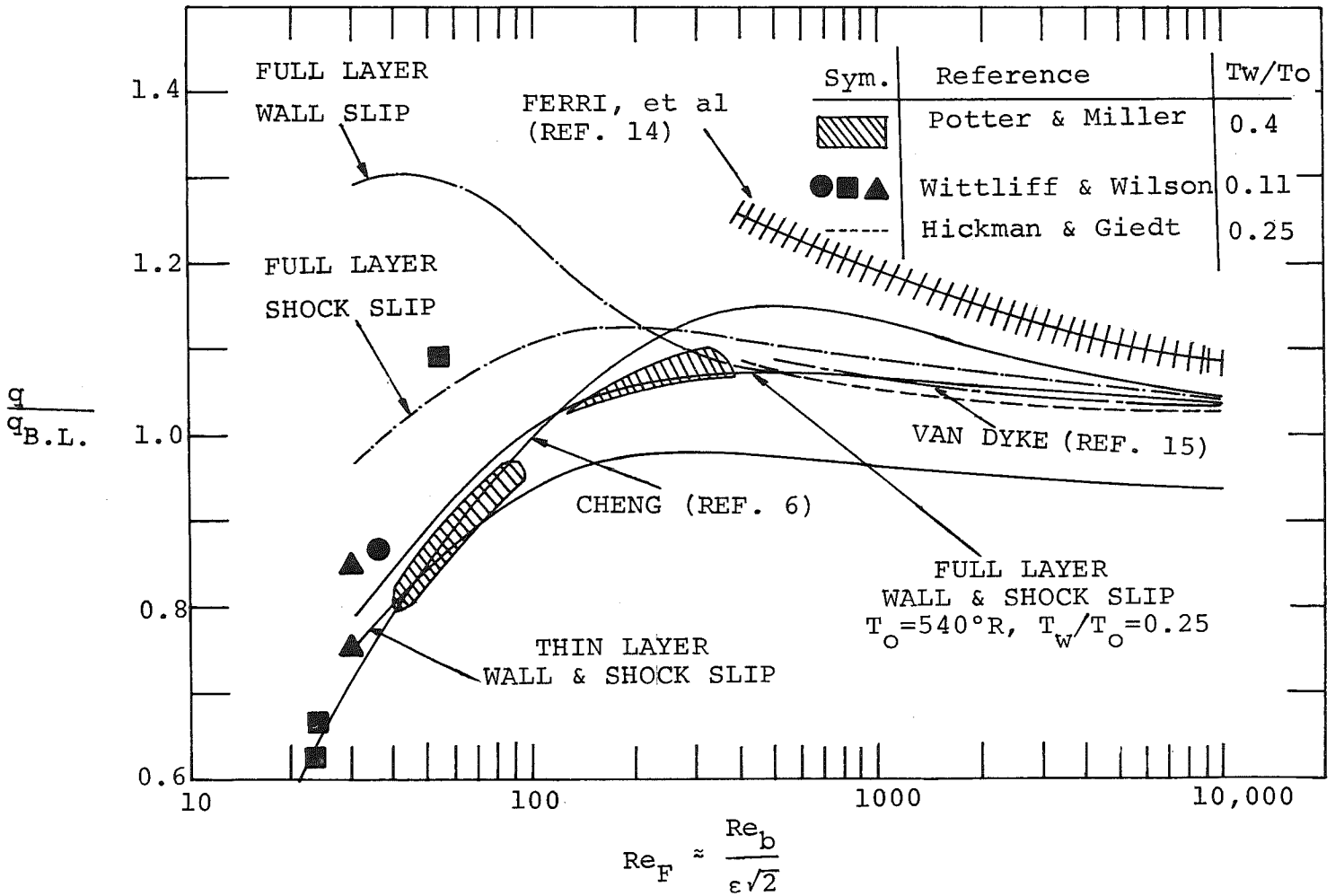

Figure 2. Stagnation point heat transfer.

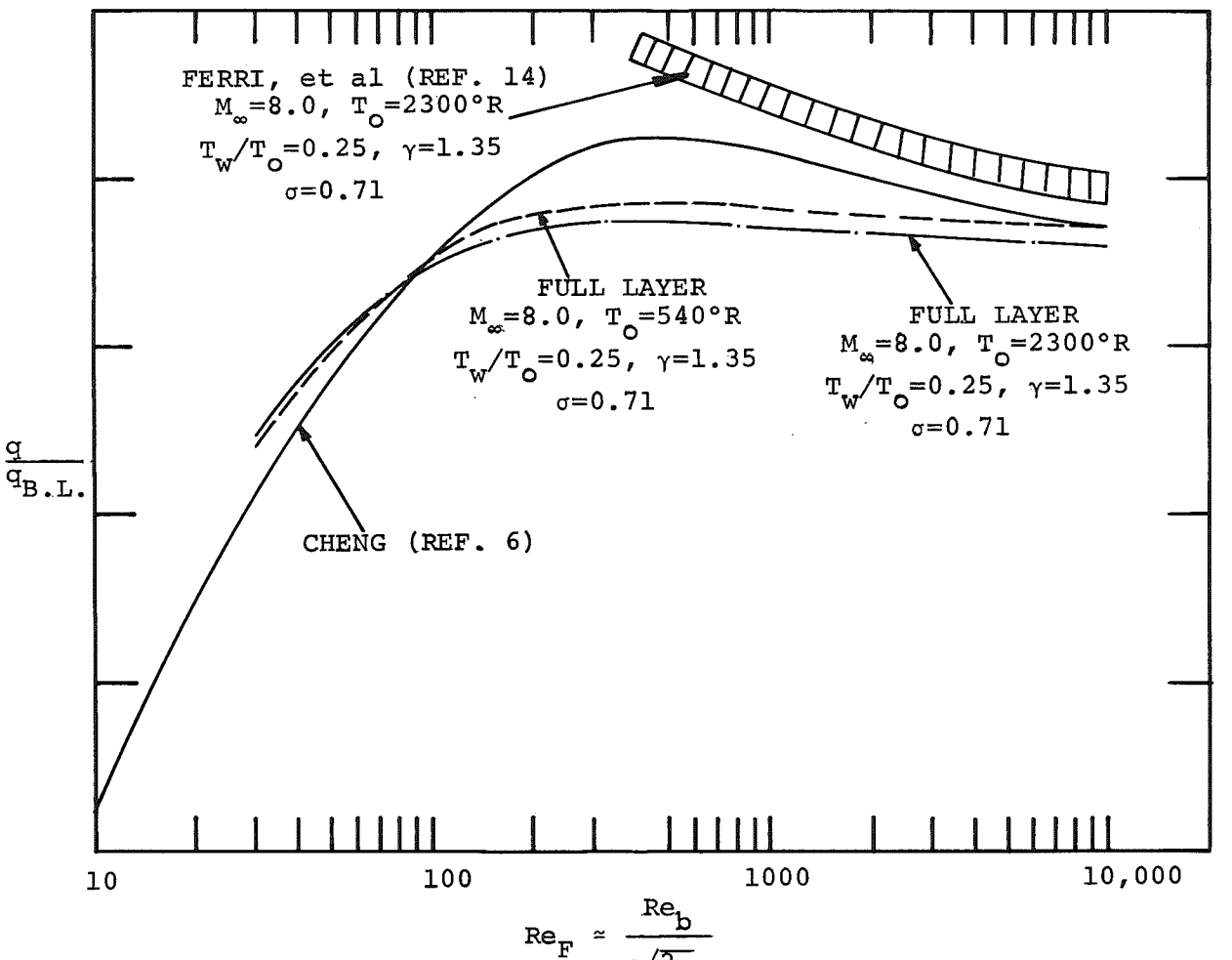

Figure 3. Further comparison of stagnation point heat transfer.

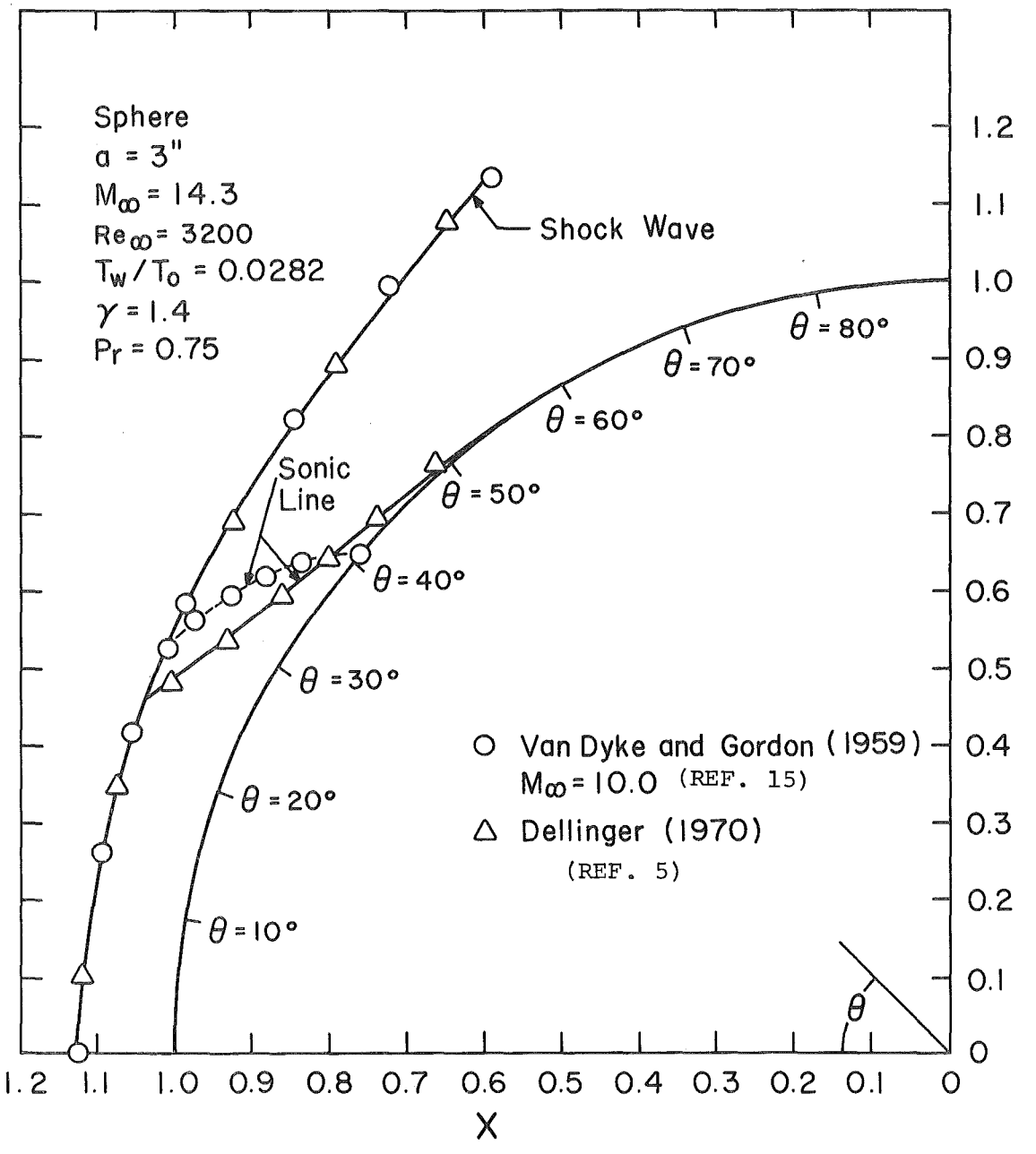

Figure 4. Shock wave and sonic line locations for a spherical body.

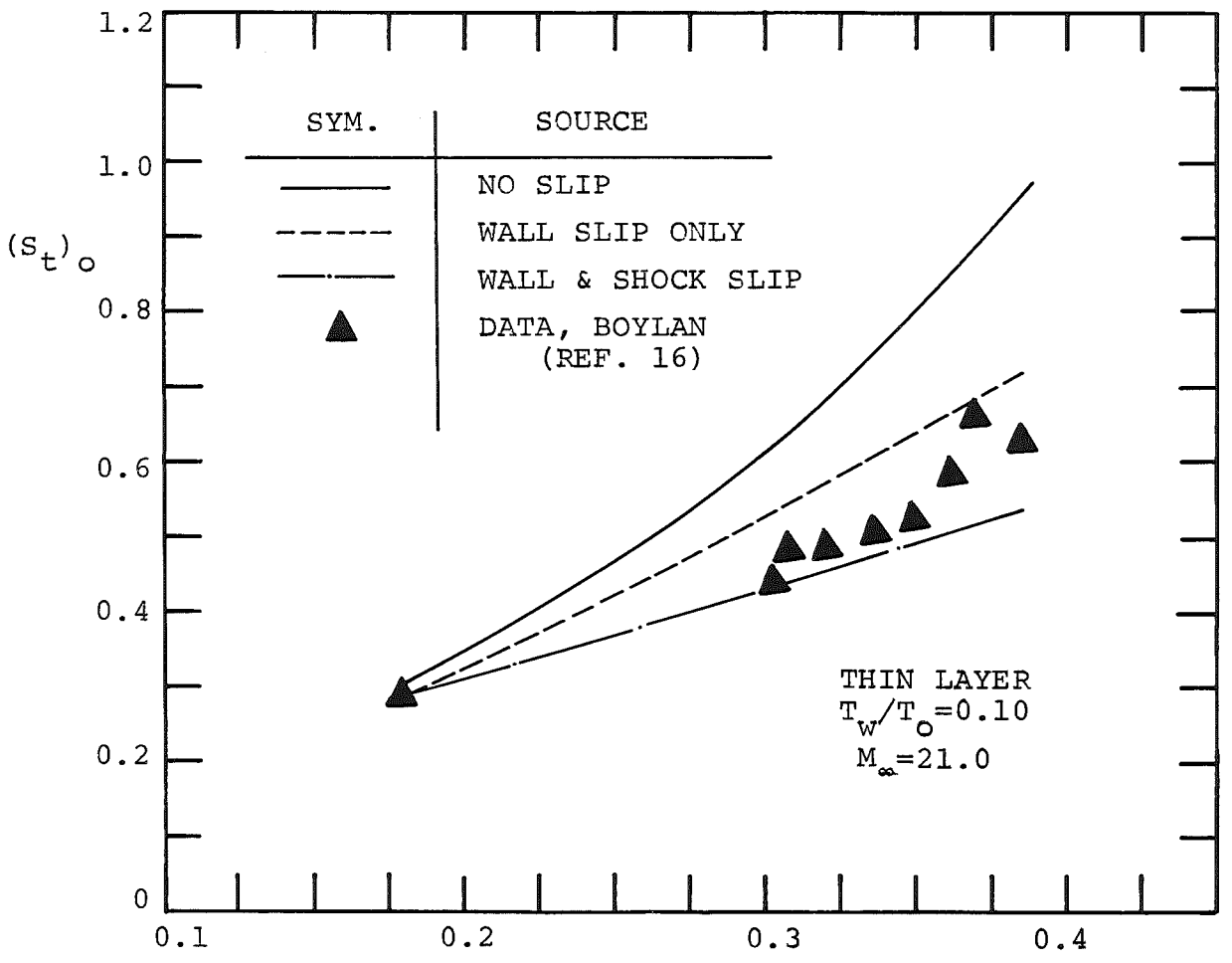

Figure 5. Variation of Stanton number with Reynolds number for thin layer.

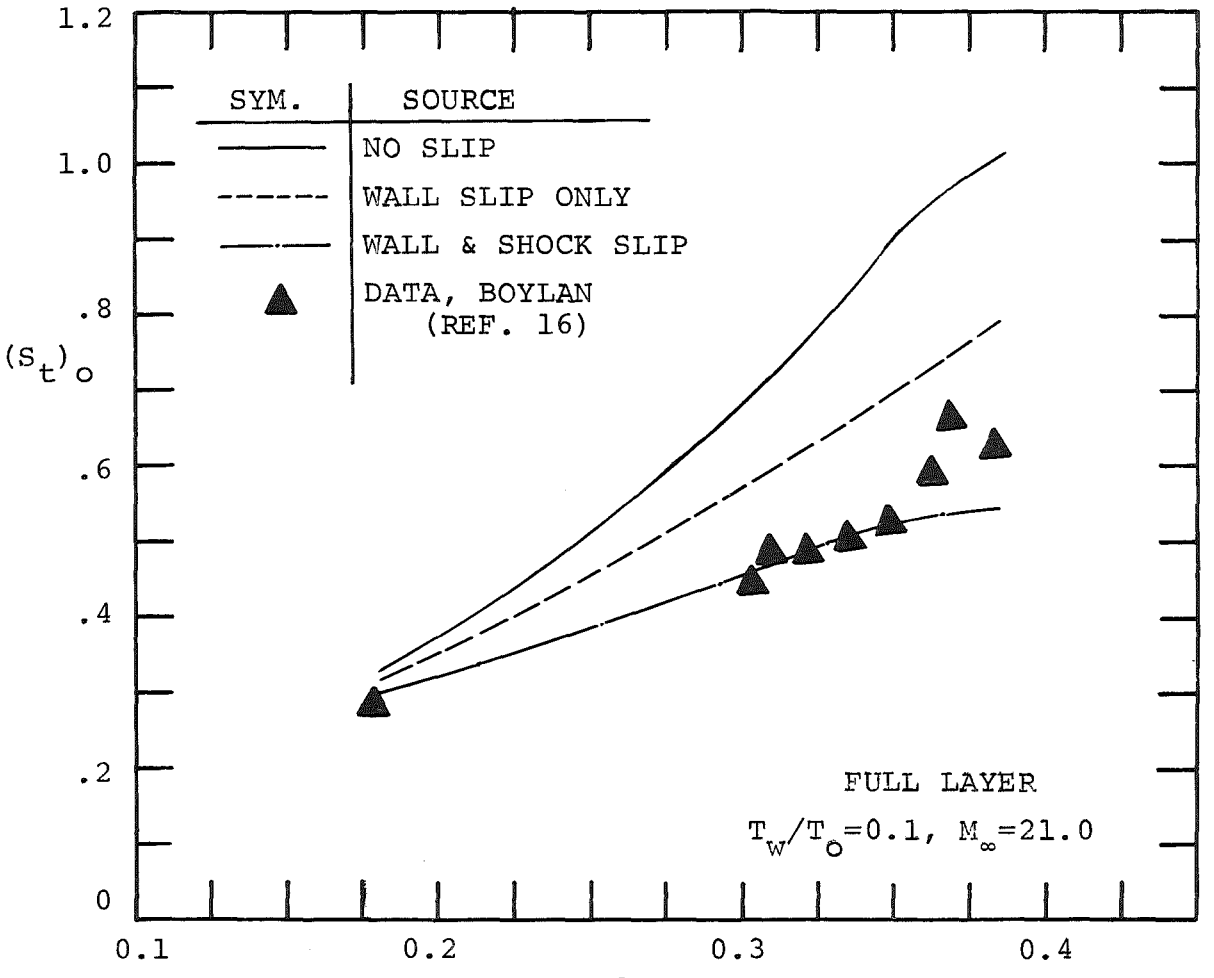

Figure 6. Variation of Stanton number with Reynolds number for full layer.

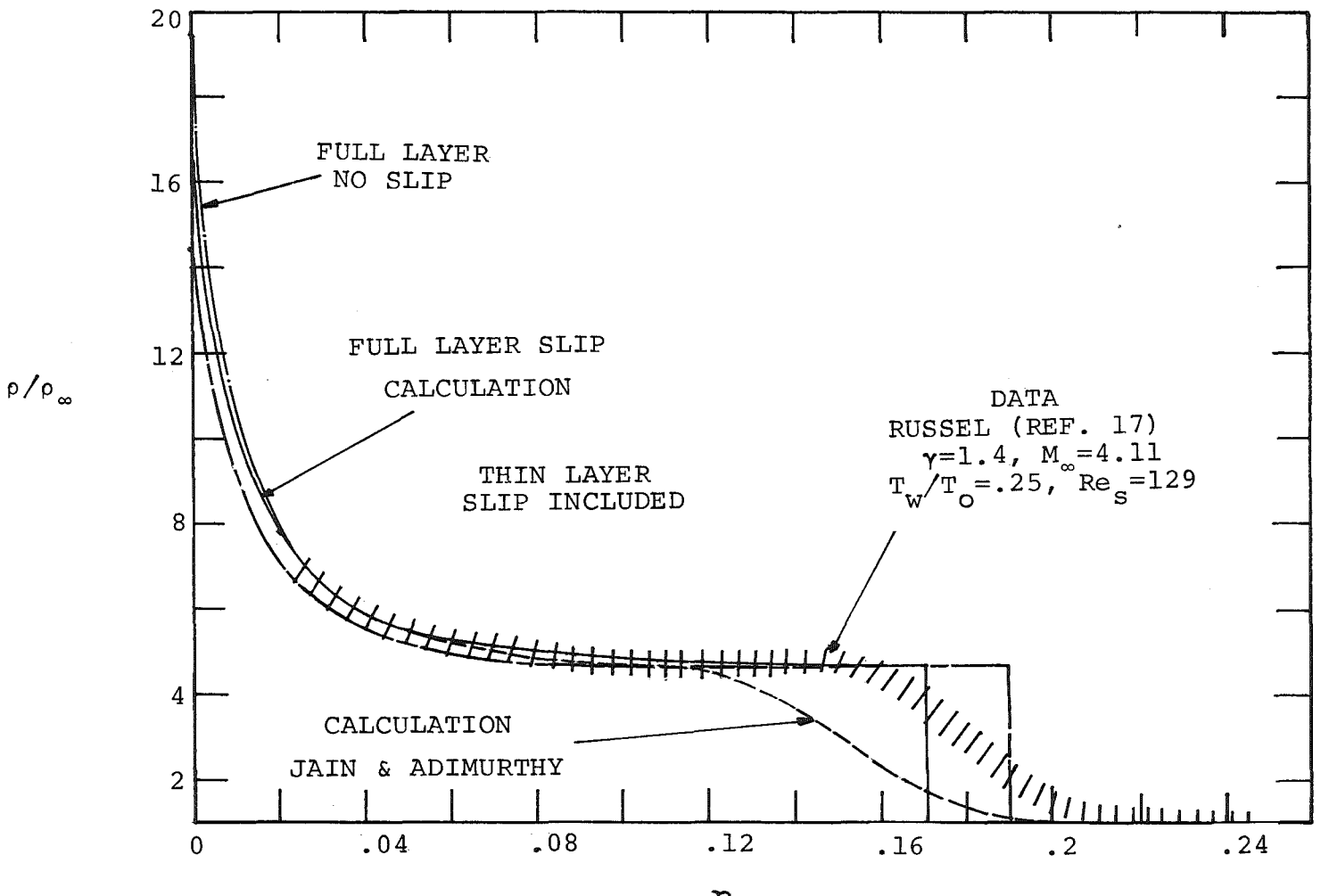

Figure 7. Stagnation point density profiles
(a) Re = 129.

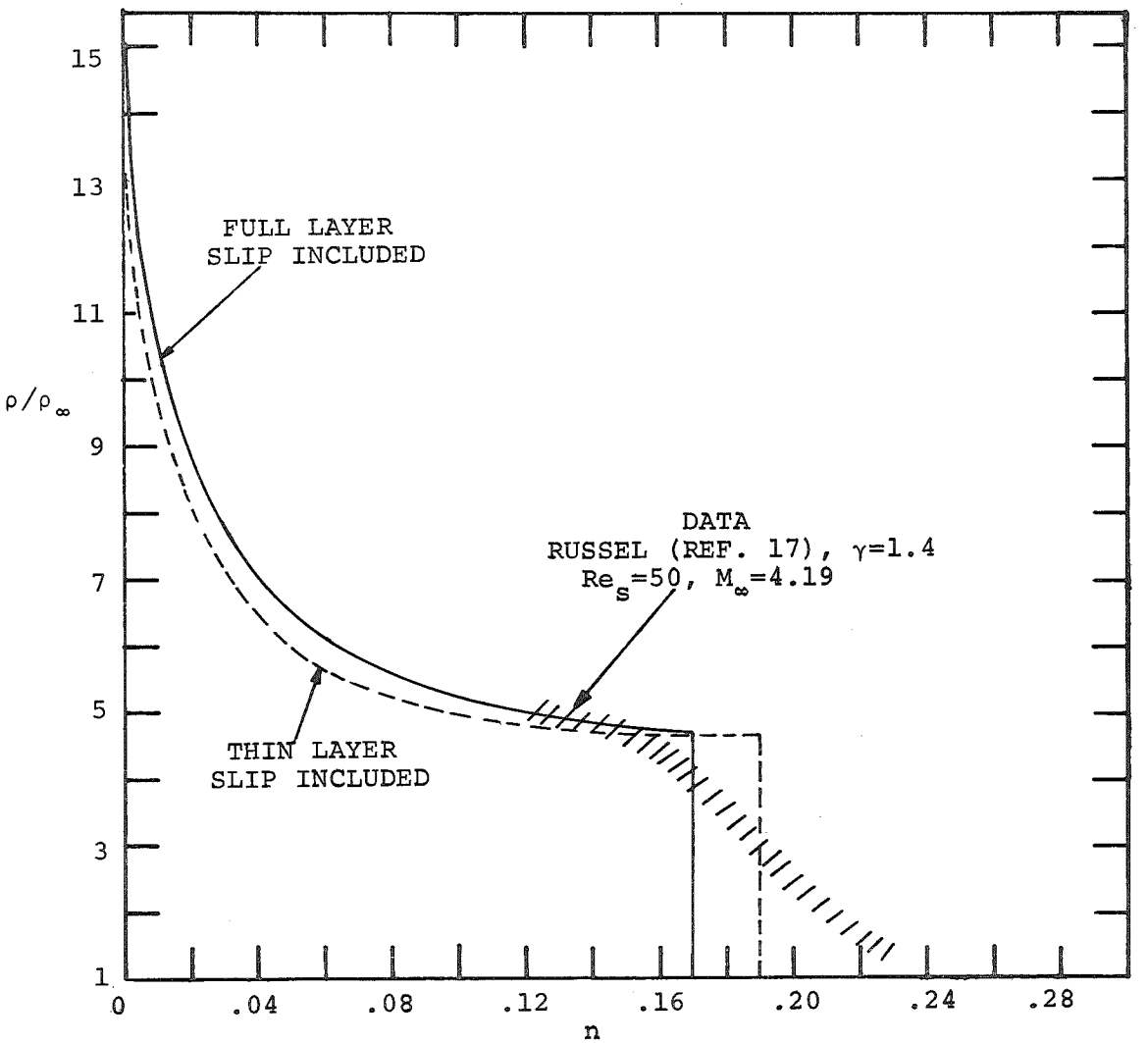

Figure 7. Stagnation point density profiles
(b) Re = 50.

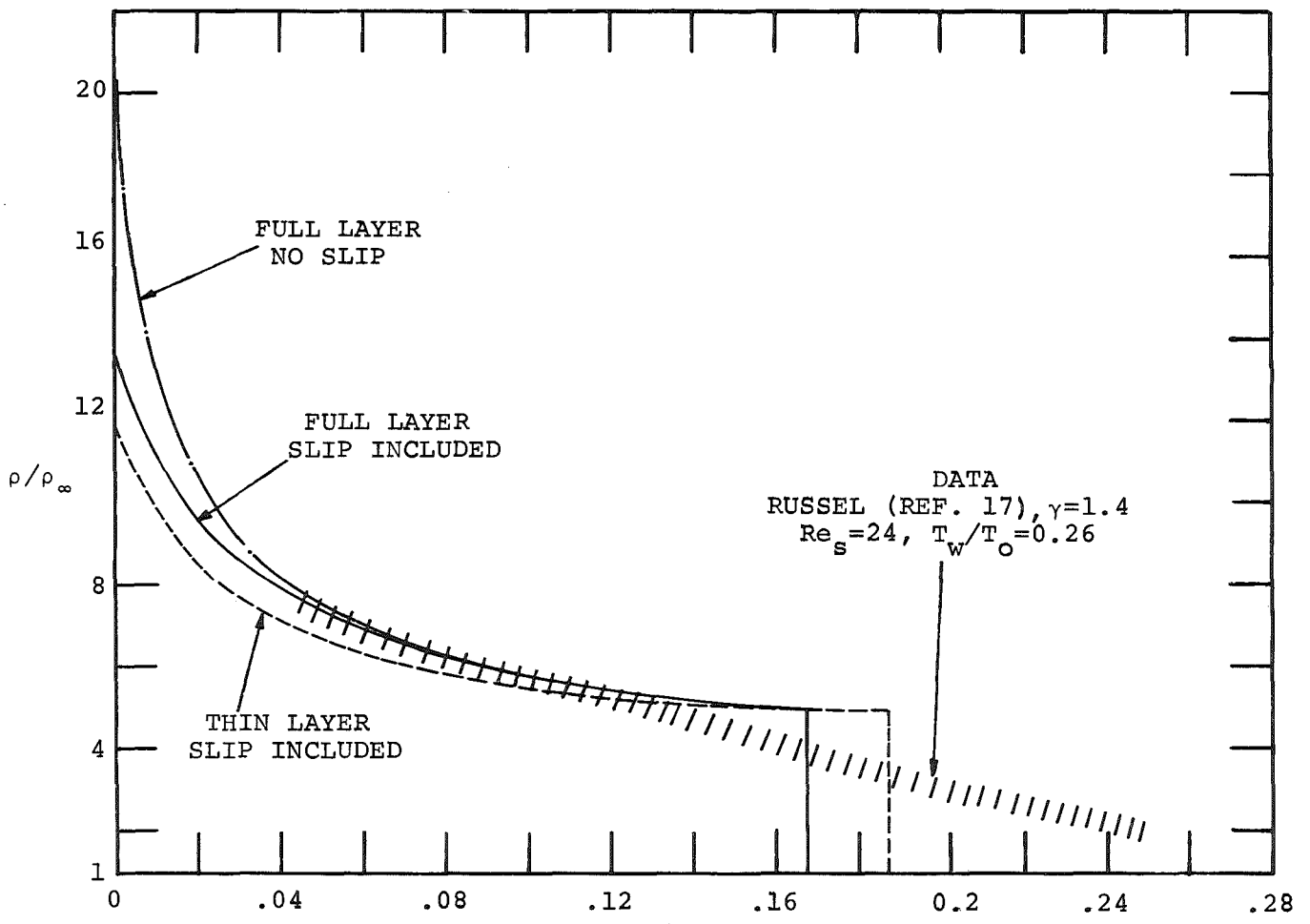

Figure 7. Stagnation point density profiles
(c) Re = 24.

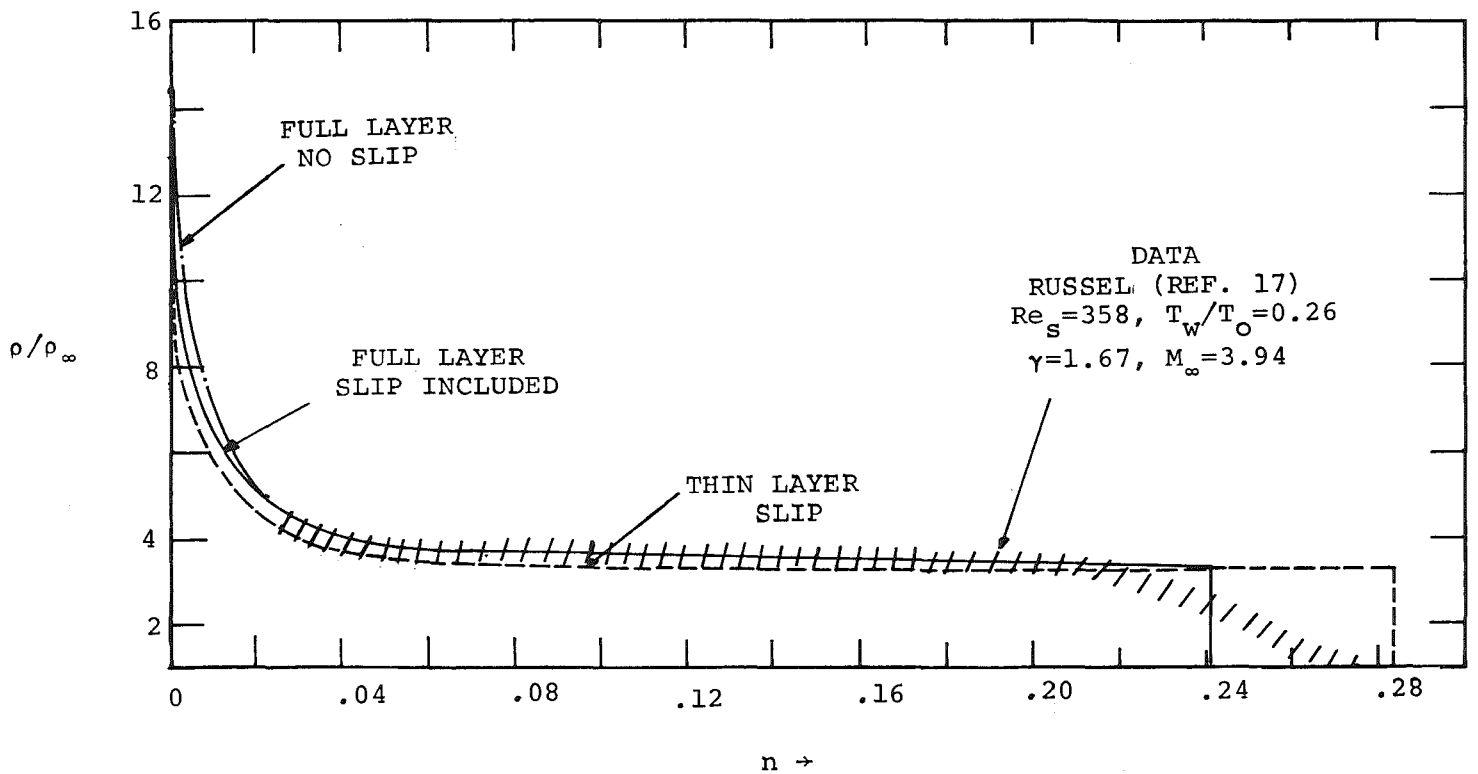

Figure 8. Stagnation point density profiles
(a) Re = 358.

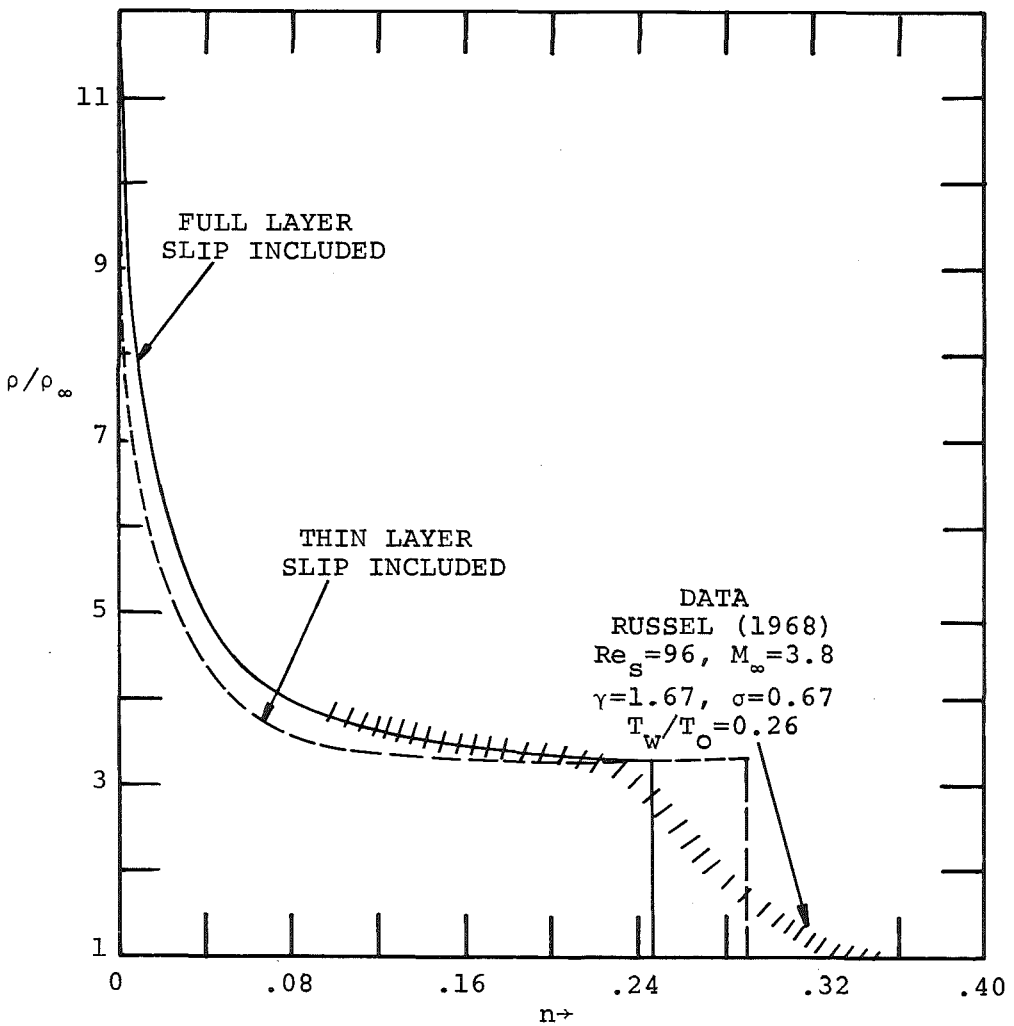

Figure 8. Stagnation point density profiles
(b) Re = 96.

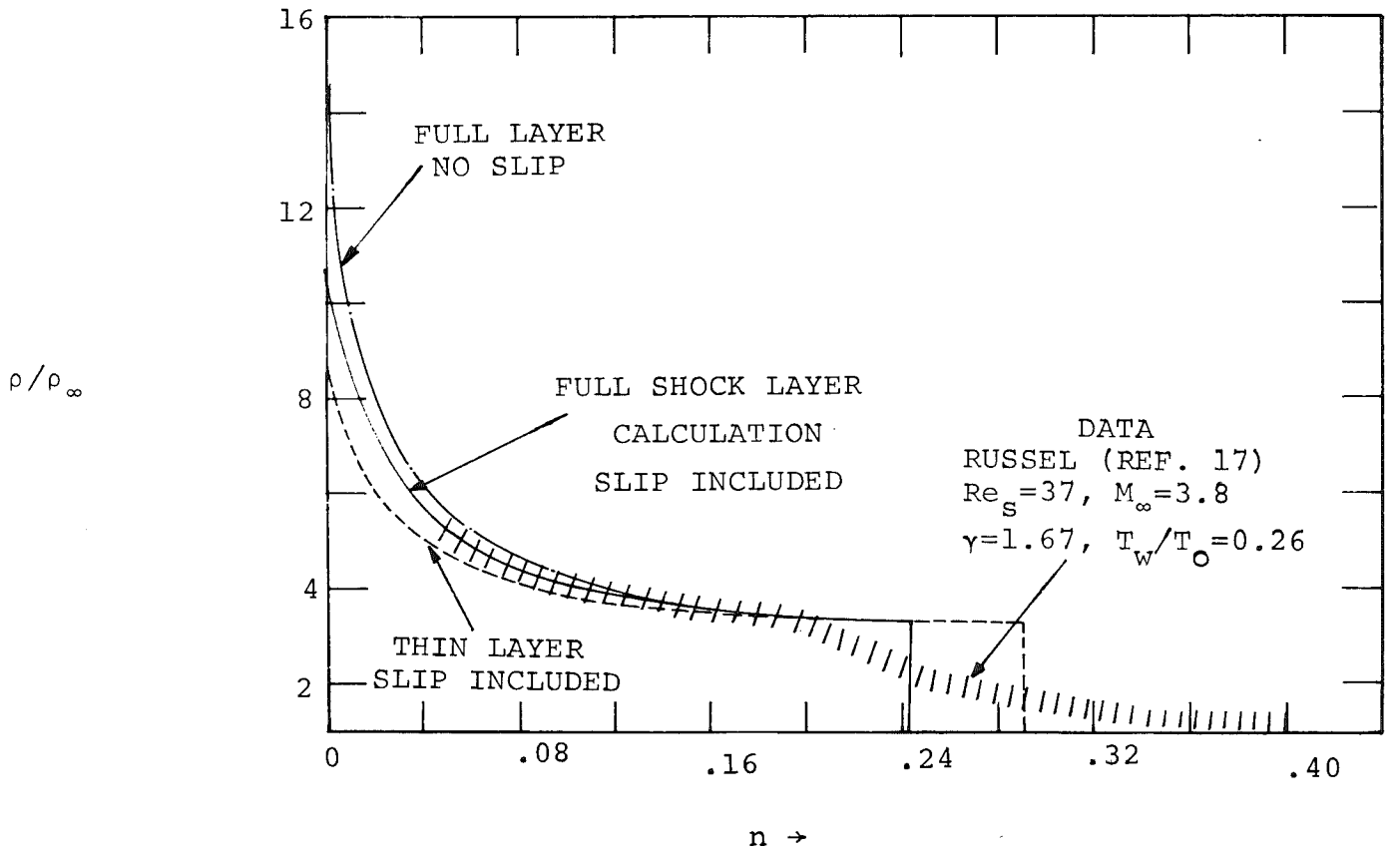

Figure 8. Stagnation point density profiles
(c) Re = 37.

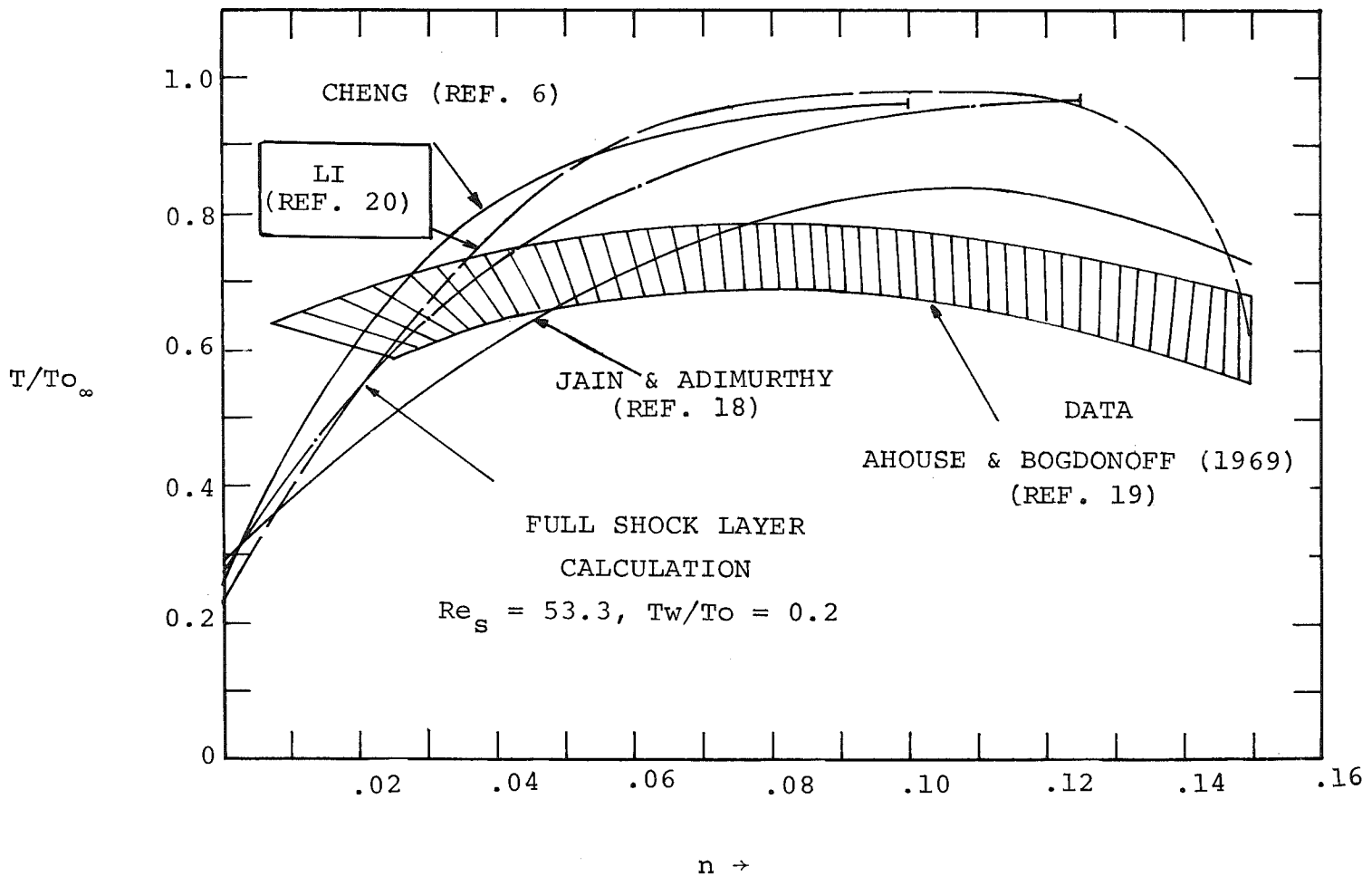

Figure 9. Stagnation point temperature profile.

LIST OF SYMBOLS

Symbol	
a	Body nose radius of curvature
a_1	Slip constant taken to be $1.2304(2-\theta_r)/\theta_r$
b_1	Slip constant taken to be $1.1750(2-\theta_r)/\theta_r$
c_1	Slip constant taken to be $2.3071(2-\alpha_t)/\alpha_t$
k	Surface curvature
M_∞	Free stream Mach number
n	Coordinate measured normal to the body, nondimensionalized by the body nose radius
p	Pressure $p^*/(\rho_\infty^* U_\infty^{*2})$
r	Nondimensional axisymmetric radius measured to a point on the body surface
Re_s	Shock Reynolds number, $\rho_{sh}^* u_{sh}^* a^*/\mu_{sh}^*$
Re_F	Defined as $Re_b/\varepsilon\sqrt{2}$, $\varepsilon = 0.13$
Re_b	Defined as $\rho_\infty^* U_\infty^* a^*/\mu_o^*$
s	Surface distance coordinate measured along the body
T	Temperature, $T = T^*/(U_\infty^{*2}/C_p^*)$
T_∞^*	Free stream temperature
u	Velocity component tangent to the body surface, (u^*/U_∞^*)
U_∞^*	Free stream velocity
u_{sh}^1	Component of velocity tangent to shock interface
v	Velocity component normal to the body surface, (v^*/U_∞^*)
v_{sh}^1	Component of velocity normal to shock interface
α	Shock angle, see Figure 1
α_t	Thermal accommodation coefficient here taken to be 1
β	Angle defined in Figure 1

Symbol

γ	Ratio of specific heats
ε	Perturbation parameter, $\varepsilon = [\mu^* (U_\infty^{*2}/C_p^*)/\rho_\infty^* U_\infty^* a^*]^{1/2}$
θ_r	Fraction of incident molecules diffusely reflected
μ	Coefficient of viscosity, $\mu = \mu^*/\mu^*(U_\infty^{*2}/C_p^*)$
ρ	Density, $\rho = \rho^*/\rho_\infty^*$
ρ_∞^*	Free stream density
τ	Shear stress, $\tau^*/(\rho_\infty^* U_\infty^{*2})$
ϕ	Body angle defined in Figure 1
σ	Prandtl number

Subscripts

1	Wall value
0	Stagnation point value
sh	Behind the shock
∞	Free stream conditions

Superscripts

*	Dimensional quantities
J	0 for plane flow and 1 for axisymmetric flow
$(\bar{\ })$	Dependent variables normalized with their respective shock values